EXAMINATION FOR INFLUENCE ASSESSMENT METHOD ON FOREST VOLUME ESTIMATE USING REMOTE SENSING AND GIS

Hisao. Ito [a,*], Susumu. Ogawa [b]

[a] Dept of geography, Graduate school of science, Tokyo Metropolitan university 1-1 Minami-Ohsawa, Hachiohji-city, Tokyo 192-0397, Japan
ito-hisao@c.metro-u.ac.jp

[b] Dept of environmental system, faculty of geo-environmental science, Rissho university 1700 Magechi, Kumagaya, Saitama, 360-0194, Japan
ogawa@ris.ac.jp

Key words: Remote Sensing, Forestry, Resources, Statistics, Calibration, Estimation, Measurement

Abstract:

Since warning of the global warming by carbon dioxide, the biomass distribution of forest has been concerned and its study has been requested. Much expectation has focused on the remote sensing corresponding to wide area. We noticed small area and estimated the spatial distribution of the forest volume using the actual GIS and remote sensing data. We comprehended the spatial distribution of the vegetation types, the geological formation, and the water cycle. Moreover, considering the seasonal change, we assessed influence and relationship between the estimated forest volume and other natural factors. The forest volume was largely influenced by the forest types.

1. INTRODUCTION

Since warning of the global warming by carbon dioxide, the biomass distribution of forest has been concerned and its study has been requested. Much expectation has focused on the remote sensing corresponding to wide area. However, many existing studies have discussed global forest distribution. We noticed small area and estimated the forest volume using the actual GIS and remote sensing data. Next, the estimated forest volume was compared with the vegetation types, the geological formation, and the water environments which may affect forest volume.

2. METHODS

The spatial distribution of forest volume (timber volume, whole volume, and biomass) was estimated by comparing the digital numbers of satellite images and actual measurement data. At first, the effects of haze and shade were reduced by Tasseled Cap correction. Next, the forest volume each small catchment was compared with the spatial distribution of the vegetation types, the geological formation, and the water cycles estimated by the satellite images, the GIS data, and the atmospheric data.

1.1 Study Area

Okutama forest area was selected as a study area and is located in the headwaters of the Tamagawa River, the western part of Tokyo. It functions for a municipal drinking-water source, river recharge, sediment run-off prevention, and water purification for Tokyo. Most Okutama forest areas exist in intensely uneven mountainous area. The altitude ranges 200m to 2000m high. First, the small catchments were divided by DEM. The Figure 1 shows study area divided to small catchments

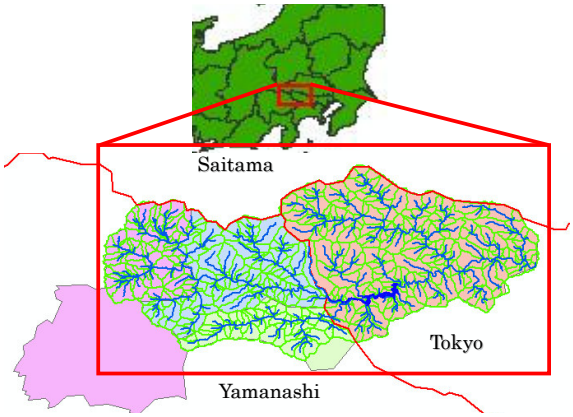

Figure 1. Study area

1.2 Data

We chose each seasonal satellite data from Landsat/TM images (Path = 107, Row = 35; Path = 108, Row = 35) and TERRA/ASTER images covering Okutama forest area. We also used a Digital Map 25000, a digital elevation model 50-m Grid (Nippon-II) produced by Japan Geographical Survey Institute, and monthly meteorological grid data made by National Digital Land Information. Moreover, we used a vegetation map and timber volume statistics (1999), breast-height diameter, height, ages, species, and the number of trees in Okutama forest area, offered by the Bureau of Waterworks of Tokyo Metropolitan Government.

* Corresponding author.

3. RESULTS

3.3 Image Pre-processing

The satellite images were corrected for atmospheric effects. First, we carried out ortho-rectification by DEM, because the study area was uneven.
Next, we reduced haze effects in the images. Equation (1) is the haze intensity of Tasseled Cap.

$$Haze = 0.846 \square TM1 - 0.073 \square TM2 - 0.46 \square TM3 - 0.0032 \square TM4 - 0.049 \square TM5 + 0.0119 \square TM7 + 0.7279 \quad (1)$$

where TMi = digital numbers for band i in the original image

The haze intensity, calculated by the equation (1), multiplied by 1.88, 0.89, 1.02, 0.85, 1.40, and 0.71 were subtracted from the original image each band except the band 6. Equation (2) shows these calculations.

$$DehazedImages = \begin{pmatrix} TM1 \\ TM2 \\ TM3 \\ TM4 \\ TM5 \\ TM6 \\ TM7 \end{pmatrix} - \begin{pmatrix} 1.88 \\ 0.89 \\ 1.02 \\ 0.85 \\ 1.40 \\ 0 \\ 0.71 \end{pmatrix} \times HazeIntensity \quad (2)$$

where Haze Intensity = Equation (1)

Next, we normalized topological effects. We did not use the existing Lambertian Reflection model or Minnaert method because we could not normalize them in this study area through the season, and then used methods judging shades by spectral characteristics. The shade intensity was judged by Equation (3), which is liner combination as well as Tasseled Cap.

$$Shade = 0.085 \square TM + 0.078 \square TM2 + 0.119 \square TM3 + 0.525 \square TM4 + 0.612 \square TM\ 5 + 0.236 \square TM7 - 39.0 \quad (3)$$

This equation was obtained by reducing effects of tree species and soils. The shade effects was normalized by Equations (3) and (4). Figure 3 compares the original and processed images.

$$Processed\ Image = \begin{pmatrix} TM1 \\ TM2 \\ TM3 \\ TM4 \\ TM5 \\ TM6 \\ TM7 \end{pmatrix} - \begin{pmatrix} 0.085 \\ 0.078 \\ 0.119 \\ 0.525 \\ 0.612 \\ 0 \\ 0.236 \end{pmatrix} \times Shade\ Intensity \quad (4)$$

3.4 Estimating Forest Volume

We used a timber volume, the whole volume, and its biomass. The timber volume data were estimated by Tokyo Metropolitan Government. The whole volume and its biomass were calculated with expansion ratios and volume density determined by each vegetation types.
Next, we carried out mixed pixel decomposition. We used Equations (5), (6), and (7), which are a liner mixed-pixel model.

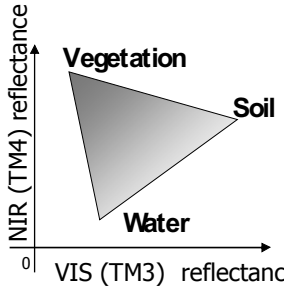

Figure 2. Feature of VIS and NIR

Figure 2 displays a distribution of VIS and NIR reflectance.

$$VIS = a_{11} \square V + a_{12} \square S + a_{13} \square W \quad (5)$$
$$NIR = a_{21} \square V + a_{22} \square S + a_{23} \square W \quad (6)$$
$$V + S + W = 1 \quad (7)$$

where a_{11} and a_{21} = reflectance of vegetation
a_{12} and a_{22} = reflectance of soil
a_{13} and a_{23} = reflectance of water

The land cover ratio for vegetation, soil, and water in a pixel was calculated by combination of these equations respectively.

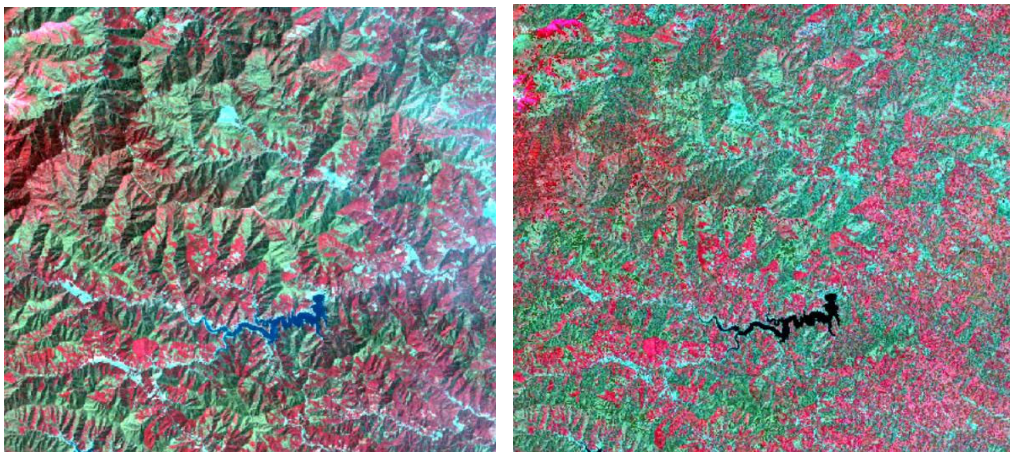

Figure 3. Original image (left) and processed image (right)

Next, the tree height was estimated from Equation (8) and the stereoscopic image made from the ASTER image. The ASTER has the stereoscopic band (backward look). The elevation values made from the ASTER were called by DSM (Digital Surface Model). Thus,

$$Tree\ height = ASTER\text{-}DSM - DEM \quad (8)$$

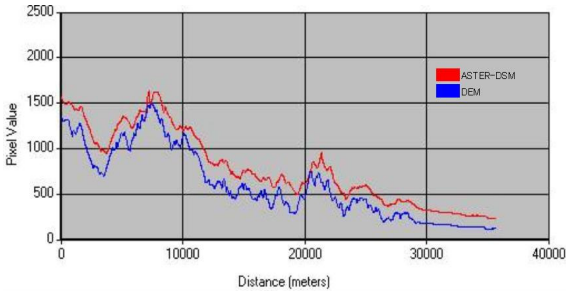

Figure 4. DSM and DEM

Figure 4 shows the cross sections of ASTER-DSM and DEM. We added pixel values of each band, NDVI, and land cover ratio each pixel in a digitized vegetation map. Figure 6 shows digitized vegetation map. NDVI was converted to 0 to 255, because NDVI include negative numbers. We carried out the regression analysis for the digital numbers each band in the satellite images vs. the timber volume, the whole volume, and the biomass. Figure 5 shows relationship between digital numbers each band and timber volumes. The correlation coefficients increased by reducing the effects of haze and shade. Table 2 shows determination coefficients between the forest volumes and estimated tree heights. Table 3 shows the determination coefficients between estimated biomass and each band, NDVI, and vegetation area summed up from land cover ratio in each pixel. Vegetation Area in Table 3 is the vegetation area summed up by the land cover ratio in each pixel. Similarly, we calculated the determination coefficients for timber volumes and whole volumes. Finally, the biomass showed the highest determination coefficient. The difference of the determination coefficient each season was recognized. Moreover, vegetation area summed up by mixed pixel decomposition was effective for estimating forest volume.

	Timber volume	Whole volume	Biomass
ASTER	0.695	0.681	0.714

Table 2. Determination coefficients of tree height and volume

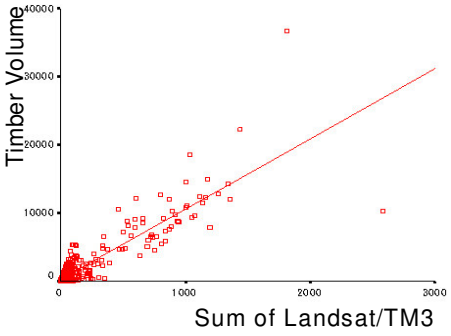

Figure 5. Relationship between digital numbers and timber volumes

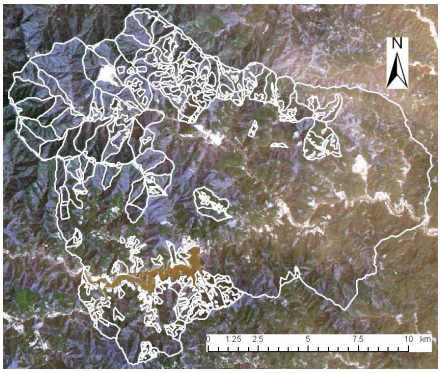

Figure 6. Digitized vegetation map

3.5 Comprehending Geological Formation

We comprehended geological formation. Slope angles and directions was calculated from DEM.

3.6 Categorizing Vegetation

Next, we categorized water area, urban area, coniferous trees, evergreen broad-leaved trees, and deciduous broad-leaved trees from Landsat/TM images. Water area, urban area, and forest area were classified with the maximum likelihood method. Moreover, in forest area, we categorized coniferous trees and broad-leaved trees. We added TM2 and TM5 on the winter season images. Higher values of this image showed broad-leaved trees and lower values of that showed coniferous trees. In the broad-leaved area, we also categorized the evergreen broad-leaved trees and the deciduous broad-leaved trees. Similarly, we added TM2 on the summer season image and TM5 on the spring season image. Higher values of this image showed deciduous broad-leaved trees and lower values showed evergreen broad-leaved trees. Figure 7 shows land cover classification and vegetation types.

	Band1	Band2	Band3	Band4	Band5	Band6	NDVI	Vegetation Area
1992/ 7/ 21	0.772	0.767	0.765	0.772	0.746	0.742	0.752	0.751
1995/ 6/ 5	0.775	0.773	0.770	0.767	0.773	0.762	0.775	0.802
1999/ 10/ 5	0.774	0.770	0.762	0.767	0.782	0.744	0.780	0.732
1999/ 12/ 23	0.775	0.775	0.775	0.756	0.775	0.763	0.773	0.728
2000/ 4/ 13	0.771	0.769	0.765	0.764	0.771	0.750	0.771	0.739

Table 3. Determination coefficients of Biomass and bands

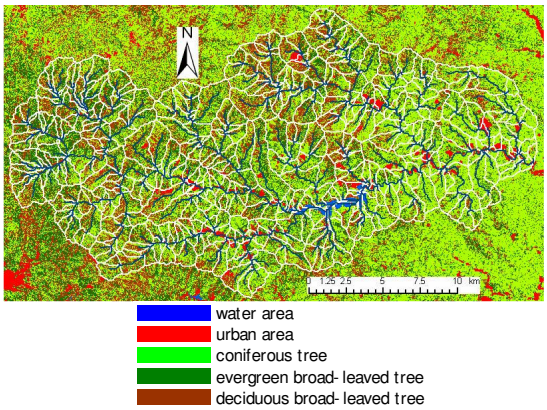

Figure 7. Vegetation types

3.7 Comprehending Water Cycle

Water cycle in forest could simply be showed as follows.

$$P = E + D + G \tag{9}$$

where P = Precipitation
E = Evapotraspiration
D = River discharge
G = Groundwater infiltration

These were calculated from the remote sensing data, the GIS data, and the metrological data respectively.
We adopted the monthly meteorological grid data for precipitation. Figure 8 shows the precipitation of the monthly meteorological grid data.

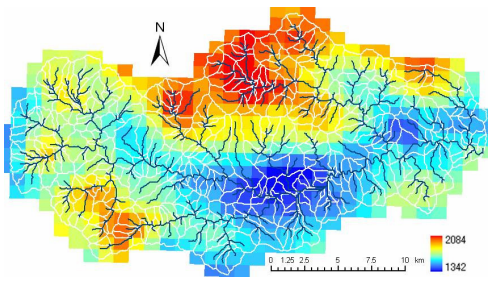

Figure 8. Spatial distribution of precipitation

Evapotranspiration was calculated by the improved Penman's method.

$$E = \frac{\Delta}{\Delta+\gamma} Q_n + \frac{\gamma}{\Delta+\gamma} f(u)(e_a^* - e_a) \tag{10}$$

$$Q_n = \frac{R_n}{L_l} \tag{11}$$

$$R_n = R_s(1-\alpha_s) + \varepsilon_s R_{ld} - R_{lu} \tag{12}$$

$$R_{ld} = \varepsilon_a \sigma T_a^{\ 4} \tag{13}$$

$$\varepsilon_a = 1.24\left(\frac{e_a}{T_a}\right)^{1/7} \tag{14}$$

$$R_{lu} = \varepsilon_s \sigma T_s^{\ 4} \tag{15}$$

where E = Evapotranspiration
$\Delta=(de^*/dT)_r$
$\gamma \equiv c_p p/\varepsilon l$,
Q_n = Available energy flux density (mm/day)
f(u) = Wind function (mm/day)
u = Mean wind-speed (m/s)
e_a^* = Saturated vapor pressure (hPa)
e_a = Vapor pressure (hPa)
R_n = Net radiation (W/m^2)
L_l = Latent heat (=2.454×10^{6}J/kg)
R_s = Short-wave radiation (W/m^2)
α_s = Albedo
R_{ld} = Downward long-wave radiation (W/m^2)
R_{lu} = Upward long-wave radiation (W/m^2)
ε_s = Emissivity of surface (=0.97)
ε_a = Atmospheric emissivity
σ= Stefan-Bolzmann constant (5.67×10^{-8} Wm^{-2}K^{-4})
T_a = Atmospheric temperature (K)
T_s = Surface temperature (K)

The albedo and the surface temperature were calculated from the Landsat/TM images. The albedo is the mean of the reflectance in the visible spectrum. Figure 9 shows the calculated spatial distribution of the albedo. The surface temperature was calculated from TM6. Figure 10 shows the estimated spatial distribution of the surface temperature. We adopted the monthly meteorological grid data for atmospheric temperature. Figure 11 shows the atmospheric temperature of the monthly meteorological grid data. Wind-speed, vapor pressure, and, short-wave radiation was used from the metrological data. In addition, short-wave radiation was used from the solar radiation. Table 4 shows metrological data used.

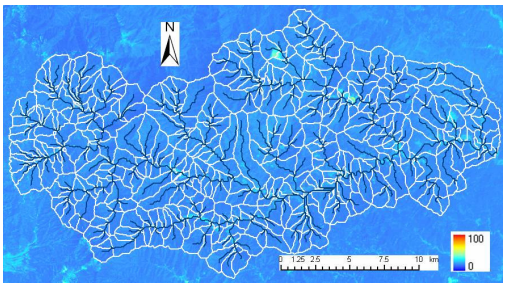

Figure 9. Spatial distribution of the albedo

	January	February	March	April	May	June	July	August	September	October	November	December
wind-speed	1.0	1.1	1.0	1.1	1.0	0.9	0.8	0.9	0.8	0.8	0.9	1.0
solar radiation	4.23	5.98	7.23	6.48	7.84	6.44	8.22	6.90	4.52	3.96	3.06	3.84
vapor pressure	6.35	3.08	8.91	8.91	12.09	16.30	34.05	41.23	21.04	14.92	10.41	6.36

Table 4. Mean values of wind-speed, solar radiation, and vapor pressure

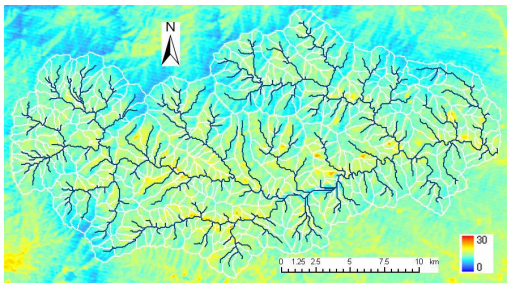

Figure 10. Spatial distribution of the surface temperature

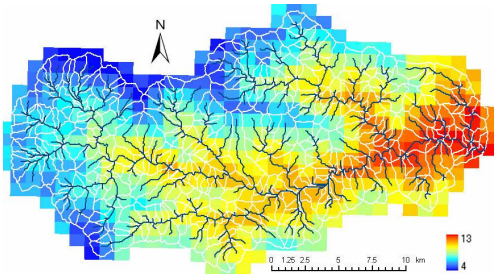

Figure 11. Spatial distribution of the atmospheric temperature

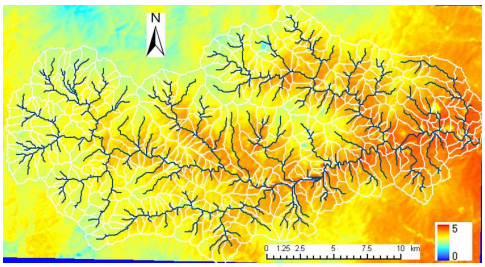

Figure 12. Spatial distribution of evapotranspiration

Next, we summed up precipitation each grid on the down slope angle for the estimate of discharge. We carried out the regression analysis between the estimated discharge and the actual observed discharge. These are applied for spatial distribution of flow in the watershed. Figure 13 shows estimated discharge.

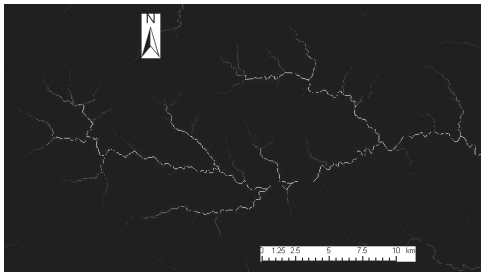

Figure 13. Added precipitation to down slope

Groundwater infiltration was calculated using precipitation, evapotranspiration, and, discharge and equation (9). The figure 14 shows calculated groundwater infiltration. The ground water infiltration was mostly effected from precipitation, because the discharge made by precipitation.

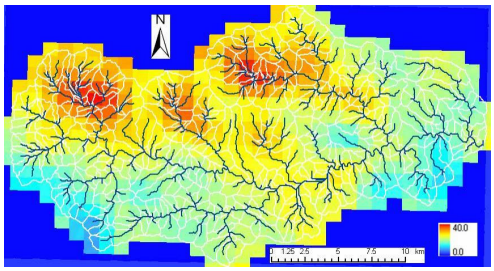

Figure 14. Spatial distribution of infiltration rate

4. DISCUSSION

In estimating forest volume, the correlation coefficients between land cover ratio in mixed pixels and estimated tree height was very high. Thus, forest volume might be estimated in higher accuracy.

The forest volume was almost independent from vegetation types, but forest volume was affected by the distribution of the vegetation types each watershed. At present, mixed forest of confusions trees and broad-leave trees seems to have the most material volume.

Vegetation types are also affected by the temperature and the precipitation. Moreover, the precipitation is affected by the forest and its evapotranspiration.

5. CONCLUSION

The mixed pixel decomposition method for remote sensing data could estimate forest volumes precisely. We obtained a spatial distribution of hydrological data in the forest using remote sensing, GIS, and meteorological data. The forest volume was mainly influenced by forest types.

ACKNOWLEDGEMENTS

This study used the ASTER data provided by ASTER announcement of research opportunity (ARO). The forest volume data and metrological data were provided by the Water Resource Management Office of the Waterworks Bureau of the Tokyo metropolitan government. We greatly appreciate for these organizations corporation.

REFERENCES

K, Saito, 2003. Estimated groundwater recharge including water pipes leakage in Kumagaya city. ACRS 2003 ISRS (The 24th Asian Conference on Remote Sensing & 2003 International symposium on remote sensing)

W. Takeuchi, 2000. Estimation of Land Cover Mixing Ratio within a Pixel by Scaling between NOAA/AVHRR and LANDSAT/TM Data. 22nd Asian Conference of Remote Sensing